sp^2/sp^3 hybridization ratio in amorphous carbon from C 1s core-level shifts: X-ray photoelectron spectroscopy and first-principles calculation

Rainer Haerle,[1,2,*] Elisa Riedo,[3,†] Alfredo Pasquarello,[1,4] and Alfonso Baldereschi[1,2]
[1]*Institut Romand de Recherche Numérique en Physique des Matériaux (IRRMA), PPH-Ecublens, CH-1015 Lausanne, Switzerland*
[2]*Institut de Physique Appliquée (IPA), Ecole Polytechnique Fédérale de Lausanne (EPFL), PHB-Ecublens, CH-1015 Lausanne, Switzerland*
[3]*Institut de Physique Expérimentale (IPE), Ecole Polytechnique Fédérale de Lausanne (EPFL), PHB-Ecublens, CH-1015 Lausanne, Switzerland*
[4]*Ecole Polytechnique Fédérale de Lausanne (EPFL), PPH-Ecublens, CH-1015 Lausanne, Switzerland*
(Received 12 June 2001; revised manuscript received 22 August 2001; published 26 December 2001)

Using a combined experimental and theoretical approach, we address C 1s core-level shifts in amorphous carbon. Experimental results are obtained by x-ray photoelectron spectroscopy (XPS) and electron-energy-loss spectroscopy (EELS) on thin-film samples of different atomic density, obtained by a pulsed-laser deposition growth process. The XPS spectra are deconvoluted into two contributions, which are attributed to sp^2- and sp^3-hybridized atoms, respectively, separated by 0.9 eV, independent of atomic density. The sp^3 hybridization content extracted from XPS is consistent with the atomic density derived from the plasmon energy in the EELS spectrum. In our theoretical study, we generate several periodic model structures of amorphous carbon of different densities applying two schemes of increasing accuracy in sequence. We first use a molecular-dynamics approach, based on an environmental-dependent tight-binding Hamiltonian to quench the systems from the liquid phase. The final model structures are then obtained by further atomic relaxation using a first-principles pseudopotential plane-wave approach within density-functional theory. Within the latter framework, we also calculate carbon 1s core-level shifts for our disordered model structures. We find that the shifts associated to threefold- and fourfold- coordinated carbon atoms give rise to two distinct peaks separated by about 1.0 eV, independent of density, in close agreement with experimental observations. This provides strong support for decomposing the XPS spectra into two peaks resulting from sp^2- and sp^3-hybridized atoms. Core-hole relaxations effects account for about 30% of the calculated shifts.

DOI: 10.1103/PhysRevB.65.045101 PACS number(s): 71.15.Mb, 71.23.−k, 81.05.Uw, 82.80.Pv

I. INTRODUCTION

The physical and structural properties of amorphous carbon (a-C) have been the subject of intense experimental[1–6] and theoretical[7–14] research for several decades. Amorphous carbon is a disordered phase of carbon without long-range order, containing carbon atoms mostly in graphitelike sp^2 and diamondlike sp^3 hybridization states. Carbon atoms in nonhydrogenated a-C films form chemical bonds by hybridization of their outermost s and p orbitals in tetrahedral (sp^3 hybridization), trigonal (sp^2 hybridization), and more rarely linear (sp^1 hybridization) spatial configurations. These configurations correspond to different coordination numbers and chemical bonds.[15] While a C atom in an sp^3 hybridization state can only form σ bonds, sp- and sp^2-hybridized C atoms can also give rise to π bonding. Since σ bonds are stronger and stiffer than π bonds, the concentration of such bonds directly determines the mechanical properties of an a-C film, such as, e.g., the hardness.[16] Experimental[1,5,6] and theoretical[8–10,12,14] studies showed that the sp^2/sp^3 hybridization ratio is linearly related with the atomic density of the a-C structure. Through the density, many other physical properties of a-C also depend on this ratio.[1,17,18] Therefore, an important parameter characterizing the quality of a-C films is the sp^2/sp^3 hybridization ratio. Depending upon the growth technique, the value of this ratio can vary over a wide range of values.[5,19]

Technological applications of a-C are numerous. They include coating materials for magnetic storage devices[16] and razor blades,[20] exploiting the high hardness, the chemical inertness, and the low friction coefficient of this material. Other applications cover antireflection coatings for optical devices, cold-field emitters in flat panel displays, and biocompatible coatings for human implants. An extended review of these properties and applications can be found in Ref. 20.

Near-edge x-ray-absorption spectroscopy (NEXAFS)[21] and high-energy electron energy loss spectroscopy (HEELS)[6,22–26] are currently considered the most reliable techniques to determine the sp^3 fraction in a-C.[5,19] These techniques determine the sp^3 fraction by comparing the intensity of a π^*-related feature in the NEXAFS or HEELS spectrum, with that of a standard 100% sp^2 film. Other techniques, including electron[27] and neutron[4] diffraction, Raman[28] and inelastic neutron[29] spectroscopies, and nuclear magnetic resonance,[30,31] are in principle sensitive to the local C configuration, but are either insufficiently accurate or unpractical for routine applications on thin films.[19] An overview of the available experimental techniques can be found in Ref. 5.

X-ray photoemission spectroscopy (XPS) on core levels stands out as a useful tool for investigating the local binding properties in materials science. Because of the localized nature of the core-level state, this measurement is mainly sensitive to the local potential. In this way, a characterization of the chemical environment of specific atoms can be given. Indeed, several investigations have made use of XPS on C 1s core levels to characterize a-C samples.[5,32–37] Carbon 1s

XPS spectra of a-C show a broad peak comprising the binding energies of graphite and diamond. The shape of the peak is found to depend on the atomic density of the amorphous sample. These observations are generally interpreted in terms of a bimodal line, whose components are associated with sp^2- and sp^3-hybridized C atoms,[5,32–36] and the relative intensity of the two contributions is assumed to measure the sp^2/sp^3 hybridization ratio.[5,33,34,36] Indeed, the ionization cross sections are independent of the chemical state of the atoms for x-ray photons with energies well above the ionization threshold.[80] However, it is not clear whether the ratio obtained in this way is reliable, and, if it matches the one determined by HEELS. Furthermore, because of the sensitivity of XPS to surface layers, it is often assumed that the ratio derived from XPS is affected by the higher sp^2 content at the surface of the films.[19]

In this work, we provide both experimental and theoretical evidence to support the reliability of the sp^2/sp^3 hybridization ratio as determined by XPS. XPS spectra are measured for thin a-C films of various atomic densities. The C 1s spectra are decomposed into two contributions and their sp^3 content is derived. This approach is validated by independent electron-energy-loss spectroscopy (EELS) measurements performed on the same samples, since this technique generally gives accepted values for the sp^3 content.[6] To establish a direct link between the XPS C 1s core-level shifts and the actual bonding configurations of the C atoms, we perform theoretical simulations. Using a tight-binding molecular-dynamics technique, we first generate several model samples of different atomic density by quenching from the melt. We then turn to a first-principles approach of higher accuracy for final structural relaxations and for a calculation of core-level shifts. This allows us to correlate core-level shifts with the hybridization of individual C atoms, which are characterized by their nearest-neighbor coordination. These results demonstrate that the C 1s core-level shifts indeed entail a hybridization of the C atoms. A partial account of the experimental results was reported previously.[36]

This paper is organized as follows. In Sec. II A, we describe the experimental setup for the XPS and EELS measurements. The analysis of the corresponding spectra is discussed in Secs. II B and II C. Section III A gives a brief overview of the theoretical methods used in this work. Section III B describes the generation of the model structures of a-C and their structural properties. In Sec. III C, the results of carbon 1s core-level shift calculations are given and discussed in relation with the experimental results of Sec. II B. Section IV concludes our work.

II. EXPERIMENT

A. Techniques

We deposited a-C films at room temperature in a pulsed-laser-deposition[38] system consisting of an ultrahigh vacuum (UHV) chamber with a base pressure of 10^{-9} Torr and a Q-switched Nd-YAG (yttrium aluminum garnet) laser with a wavelength of 532 nm, a pulse duration of 20 ns, and a frequency of 10 Hz. The distance between the target and the substrate was 3 cm. The diameter of the laser spot on the target was about 600 μm. We used silicon wafers, cleaned with acetone, as substrates for deposition. A detailed description of the experimental setup, used for the growth of the a-C thin films, is given in Ref. 36.

Four different a-C films were grown with laser fluences of $I_L=1$, 5, 12, and 35 J/cm^2. These laser fluences were chosen in order to grow samples of different atomic densities. In fact, according to the subplantation model, the density of a-C thin films depends primarily on the mean ion energy used for deposition,[39,40] which increases with I_L in the present range of fluences.[41]

Immediately after the deposition process, the samples were loaded into a different UHV system, for XPS and EELS studies at room temperature and at a base pressure of 1×10^{-10} Torr. The C 1s core-level spectra were measured using an Al $K\alpha$ 1486.3-eV x-ray source. During the measurements we did not observe any shift in the spectra indicating charging effects. The resulting experimental resolution, including the width of the x-ray line and the energy resolution of the analyzer, was about 1.1 eV. To calibrate the scale of the binding energies, we used the Si 2p core-level line of an uncovered part of the silicon substrate, which we set at a value of 99.4 eV.[42] Taking into account the relative intensities of the O 1s and C 1s peaks with their sensitivity factors,[42] we found an oxygen contamination of only 3% for all the a-C samples.

EELS measurements were performed using an EG5 VSW Scientific Instruments electron gun with an electron energy of 2057 eV. At this high energy, the penetration depth is about 4 to 8 nm, ensuring sensitivity to the bulk of the a-C films. The energy losses were studied up to 60 eV, covering the range of the plasmon peaks in a-C. In this experimental setup, we measured a width of 2 eV for the elastic peak. For both EELS and XPS measurements a hemispherical mirror analyzer was used.

B. C 1s photoelectron spectra

We obtained C 1s photoelectron spectra for each of our four samples. All the spectra show an asymmetric broad line, whose maximum shifts to higher binding energies for increasing laser fluences. Two of these spectra, corresponding to the a-C samples grown at $I_L=1$ and 12 J/cm^2, are shown in Fig. 1. The C 1s core-level spectra can be decomposed into two components.[33,36] Because the C 1s line in graphite occurs at lower binding energy than in diamond, we attribute the component at lower binding energy to sp^2 hybridization, and that at higher binding energy to sp^3 hybridization. We fitted the sp^3 component to a convolution of Gaussian and Lorentzian functions. The Gaussian component accounts for the instrumental broadening, the chemical disorder and the phonon interaction, while the Lorentzian function accounts for the finite lifetime of the core hole in the photoionization process. The sp^2 component was fitted to a Doniach-Sunjic function,[43,44] i.e., a convolution of a Gaussian and a Lorentzian with an additional parameter allowing for asymmetry in the line shape. This function is used to account for the asymmetric line shapes resulting from the screening due to

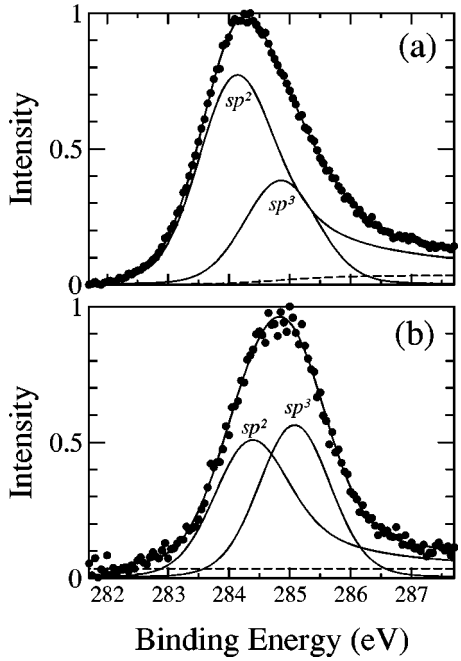

FIG. 1. Measured C 1*s* photoelectron spectra of two *a*-C films grown with laser fluences of (a) 1 and (b) 12 J/cm^3. The Shirley background and the sp^2 and sp^3 components resulting from the fit are also shown. The resulting fit is superimposed on the data.

electron-hole pair excitations at the Fermi energy,[45] and was used previously in the context of *a*-C films[33] and CN films.[46]

We fixed the Lorentzian lifetime width for both components at 215 meV.[33,45] Hence the C 1*s* spectra were fitted with nine parameters: two for defining a Shirley background proportional to the integrated peak intensity,[47] the binding energies, intensities, and widths of the two components, and, in addition, the singularity index of the Doniach-Sunjic function for the sp^2 component. The sp^2/sp^3 hybridization ratio is then derived from the relative intensities of the two components. We found that the sp^3 content increases with laser fluence, in accord with the expected dependence on atomic density.[5,6,40] The separation between the two components in the four C 1*s* spectra is almost constant, the average separation being 0.90 eV with an error of 0.05 eV. The fit gives Gaussian widths [full widths at half maximum (FWHM's)] of 1.25 ± 0.05 eV for the individual components in the spectra. The instrumental broadening being 1.1 eV, these larger widths should be attributed to chemical disorder and phonon broadening. The singularity index is found to range between 0.14 and 0.18. The relevant parameters resulting from the fit for the four *a*-C films are given in Table I. The separation between the sp^2 and sp^3 peaks, the Gaussian widths, and the singularity parameter are in excellent agreement with previous measurements.[33] The decomposition into individual sp^2 and sp^3 peaks is illustrated in Fig. 1 for two of our samples.

Because of the large number of free fitting parameters, our fitting procedure gives large errors on the binding energies of the sp^2 and sp^3 peaks and on their relative intensities. However, these errors can be significantly reduced by considering only fits with physically meaningful parameters.

TABLE I. Results derived from measured C 1*s* XPS spectra for samples grown with different laser fluences (I_L): the separation Δ^{expt} between sp^2 and sp^3 components, the percentage N_{sp^3} associated with the intensity of the sp^3 component, and the atomic density ρ calculated using Eq. (2) from Ref. 6. The errors are discussed in the text.

I_L (J/cm^2)	Δ^{expt} (eV)	N_{sp^3} (%)	ρ (g/cm^3)
1	0.91 ± 0.05	34 ± 10	2.39 ± 0.14
5	0.83 ± 0.08	50 ± 3	2.61 ± 0.04
12	0.86 ± 0.09	53 ± 5	2.65 ± 0.07
35	0.87 ± 0.08	63 ± 6	2.78 ± 0.08

In fact, only fits yielding two Gaussian functions with FWHM's larger than our resolution (1.1 eV) should be accepted. The FWHM's of the sp^2 and sp^3 components turn out to be close to each other for most of our samples. To provide a reasonable estimate of the involved errors, we therefore performed a second set of fits imposing equal FWHM's for both components.[48] With respect to the fit with free parameters, the procedure gives fits of equivalent quality and essentially unmodified parameters (Table I), but reduces the errors considerably. We found errors up to 0.08 eV for the individual binding energies and up to 0.09 eV for the separation between the two peaks. The errors in the intensities result in an uncertainty of at most 0.10 on the determined sp^3 fractions (Table I).

Mizokawa *et al.* found a separation of 0.8 eV between the positions of the C 1*s* XPS lines in graphite and diamond,[49] in good agreement with the separation of 0.9 eV between sp^2 and sp^3 peaks found for *a*-C films in the present work, as well as in Refs. 32 and 33. However, when the C 1*s* binding energies in graphite[45] and diamond[50] are taken from two independent measurements, a separation of 0.6 eV is found. At present, the origin of this discrepancy is unclear. We note that, even assuming that the structural disorder induces only line broadening, the separation between sp^2 and sp^3 peaks in amorphous carbon and between the positions of the C 1*s* line in diamond and graphite do not necessarily have to match. In fact, while the former separation is an intrinsic bulk property, the latter can depend on surface effects.

C. Density and sp^3 fraction from EELS

To assess the sp^3 hybridization content of our samples independently of XPS, we performed EELS measurements on two of them, those grown with $I_L=1$ and 12 J/cm^2. The corresponding EELS spectra are shown in Fig. 2. From the position E_p of the $\sigma+\pi$ plasmon peak in the low energy-loss spectra, we derive the atomic density ρ of the *a*-C film using the quasifree electron model, which gives the relationship[51]

$$E_p=\hbar\left(\frac{n_e e^2}{\epsilon_0 m^*}\right)^{1/2}, \tag{1}$$

where n_e is the valence electron density, m^* is the effective electron mass, and ϵ_0 is the static dielectric constant. Re-

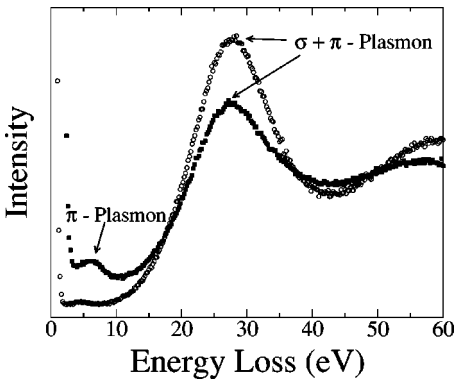

FIG. 2. Measured EELS spectra of two *a*-C films grown with laser fluences of 1 (solid squares) and 12 (empty circles) J/cm^3. These measurements were obtained with an energy of the primary electron beam of 2057 eV.

cently, a comparison with x-ray reflectivity measurements demonstrated that this procedure can give reliable values of the atomic density of carbon materials.[6] To this end, m^* should take a value of $0.87m_e$, where m_e is the free-electron mass.[6] From the EELS spectra in Fig. 2, we derived atomic densities $\rho=2.37\pm0.07$ and 2.58 ± 0.07 g/cm^3 for the films grown with $I_L=1$ and 12 J/cm^2, respectively.

The relation between atomic density and sp^3 fraction is well documented in the literature.[5,6,8–10,12,14] To obtain the sp^3 fraction N_{sp^3} from the density ρ determined by EELS, we use the relation

$$N_{sp^3}[\%]=\frac{\rho[\mathrm{g/cm^3}]-1.92}{0.0137} \tag{2}$$

derived by Ferrari *et al.* using accurate HEELS measurements.[6] We determined sp^3 fractions of 0.33 ± 0.05 and 0.48 ± 0.05 for samples grown with $I_L=1$ and 12 J/cm^2, respectively. These values compare very well with the fractions 0.34 ± 0.10 and 0.53 ± 0.05 derived for the same samples from the intensities in the x-ray photoelectron spectra (see Table I). This good agreement provides strong evidence of the soundness of the sp^3 fractions determined by XPS. In particular, XPS results have long been considered unreliable due to their sensitivity to surface layers.[5] Because of the different penetration depth of XPS (2.7 nm) and EELS (5 nm) measurements,[52] our results show that, at least for the sp^3 fractions considered here, surface effects play a minor role.

III. THEORY

A. Methods

In our theoretical study, we generated model amorphous structures by applying in sequence two quantum-mechanical approaches of increasing accuracy. We first performed extensive molecular-dynamics simulations using an environmental-dependent tight-binding (ED-TB) Hamiltonian,[53] which provides a simple, yet accurate, quantum-mechanical description of the chemical bonds. This Hamiltonian is based on an orthogonal minimal basis set including only *s* and *p* orbitals, whose matrix elements are obtained from a fit to first-principles calculations.[53] For molecular-dynamics calculations, forces on atoms were derived by direct diagonalization of the ED-TB Hamiltonian matrix. In many applications,[12,13,15] this description proved to be more accurate than those obtained with a two-center tight-binding Hamiltonian[12,54] or with empirical potentials.[55]

The resulting model structures were subsequently relaxed further using a damped first-principles molecular-dynamics scheme based on density functional theory.[56,57] The exchange and correlation energy was accounted for by the generalized gradient approximation introduced by Perdew and Wang.[58] Only valence electrons were treated explicitly, while core-valence interactions were described by pseudopotentials. We used an ultrasoft pseudopotential for C obtained with core radii of 1.25 bohr and with two reference energies in the *s* and *p* angular momentum waves.[59] The valence wave functions and the augmented electron-density were expanded in plane-wave basis sets defined by cutoff energies of 24 and 150 Ry, respectively. The Brillouin zone was sampled using only the Γ point, which is appropriate for the large unit cells used here to model the amorphous systems with the supercell technique.

The C 1*s* core-level shifts were calculated using a first-principles scheme which includes core-hole relaxation effects.[60,61] For each atom, we performed a total-energy calculation in which the corresponding pseudopotential was replaced by one which simulates the presence of a screened 1*s* hole in the core. In these calculations, the charge neutrality required by the periodic boundary conditions was achieved by adding a uniform negative charge. By taking total-energy differences, we then obtained *relative* C 1*s* core-level energies. However, absolute extraction energies cannot be determined with this approach.

The present methodology was successfully applied to Si 2*p* (Refs. 62–68), N 1*s* (Refs. 69–71) and C 1*s* core-level shifts[72–74] in a variety of systems. In particular, Palma, Pasquarello, and Car[72] calculated C 1*s* core-level shifts within the same pseudopotential scheme as used here for a series of small molecules, including CO, CH_4, C_2H_2, and HCHO, and found them to agree closely with experiment[75] as well as with all-electron calculations.[76] We repeated these calculations using a simple cubic supercell with a lattice size of 24 a.u. and the plane-wave basis sets described above. Despite different technical ingredients, our results very closely reproduced the results in Ref. 72. We then extended this set of molecules to include CH_3CCH, and found the same level of accuracy for its three different C 1*s* shifts. The comparison between calculated and measured[75] results for this molecule is given in Table II.

In our calculations, we considered only vertical transitions, in which the atomic positions do not relax upon photoexcitation. Recently, Travaly, Gonze, and Vanderbilt showed that in polyethylene terephthalate the agreement between theory and experiment improved when including atomic relaxation.[74] However, given the excellent agreement between theory and experiment found for the test molecules in the vertical transition scheme, we did not investigate such adiabatic effects further.

TABLE II. Comparison between calculated and measured C 1*s* core-level shifts for CH_3CCH. The shifts (in eV) are given with respect to the C 1*s* level in CO. The C atom to which the calculated shift refers is indicated as C*. Experimental results are from Ref. 75.

Molecule	Theory (eV)	Expt. (eV)
C^*H_3CCH	4.69	4.40
CH_3C^*CH	5.42	5.10
CH_3CC^*H	6.03	5.80

B. Model structures of *a*-C

Our investigation covers *a*-C structures with atomic densities ranging from 1.8 to 3.0 g/cm^3. We simulated *a*-C at atomic densities of 1.77, 2.21, and 2.63 g/cm^3 by three model structures containing 128 atoms in a periodic cubic cell. In addition, we considered a series of five smaller model structures with 64 atoms in the supercell.

The first step of our generation process relies on a molecular-dynamics technique in which the interactions are described by the ED-TB Hamiltonian.[53] For each model system, we started our simulation from a well-equilibrated melt at 6000 K. Then we quenched the system in about 15 ps down to a temperature of 0 K at a constant rate of ≈ -400 K/ps. We note that the quench rate adopted here is adequate for simulating the situation of a ''thermal spike,'' which occurs when a high-energy C atom hits the surface during growth in a chemical vapor deposition process.[77]

The resulting model structures were then further relaxed within a first-principles density-functional-theory scheme.[57] Upon this relaxation, only minor readjustments of the atomic positions were observed. Only on a few occasions the coordination of a pair of atoms changed as a result of bond elongations. In Fig. 3, we illustrate the relaxed structures of the three 128-atom models using a ball and stick representation.

Nearest-neighbor coordination was obtained using a hard-sphere cutoff of 1.9 Å. This cutoff falls in a well-defined gap of the pair correlation function which occurs beyond the shell of first neighbors. The percentage of threefold- and fourfold-coordinated atoms obtained for our model structures are reported in Table III. Figure 4 shows that the fourfold percentage in our model structures increases with atomic density, in fair agreement with the empirical relation from Ref. 6. Our calculated relation between fourfold percentage and density is also in good agreement with other theoretical investigations.[11–14] In particular, it agrees well with that found for model structures of much larger size containing up to several thousand atoms, generated with the same ED-TB Hamiltonian as used here.[12,78] Note that the low fourfold percentage found for the model at $\rho = 2.15$ g/cm^3 results from the formation of graphitelike sheets, and might be affected by the small size of the simulation cell.[10]

The structural properties of our models give a picture of the *a*-C network which is consistent with experimental data[2–4] and other theoretical descriptions.[11–14,78] Table III gives relevant structural parameters of our models, such as nearest-neighbor distances and ring statistics. The average

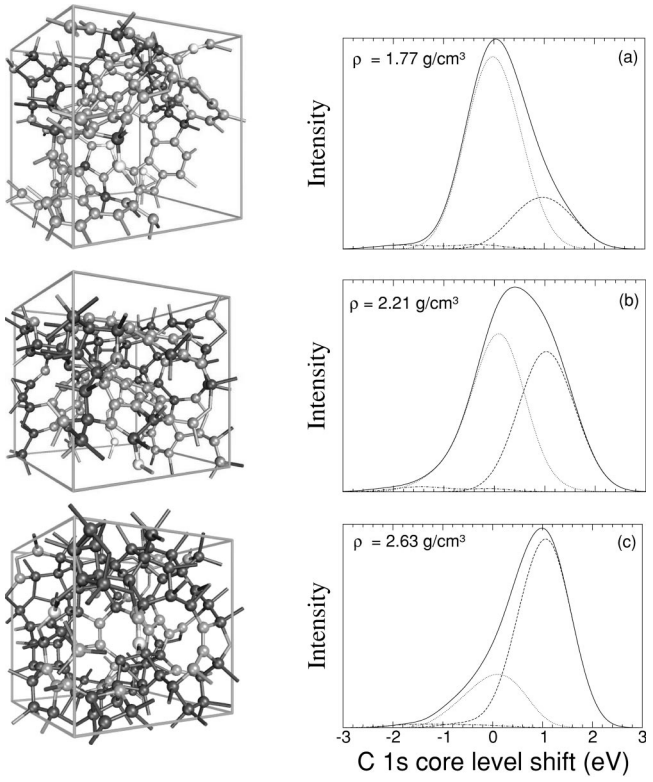

FIG. 3. Ball-and-stick representation and corresponding simulated C 1*s* core-level spectra for the three 128-atom model structures of *a*-C generated in this work, with atomic densities of (a) 1.77, (b) 2.21, and (c) 2.63 g/cm^3. In the ball and stick models, black, gray, and white atoms indicate fourfold, threefold, and twofold coordinations, respectively. The simulated spectra (solid line) are decomposed into contributions arising from twofold- (dash-dotted line), threefold- (dotted line), and fourfold- (dashed line) coordinated atoms. A Gaussian broadening of 1.0 eV is used.

nearest-neighbor distance (d_{NN}) is found to increase with atomic density, along with the average coordination number. To understand this behavior, it is useful to consider the bond lengths connecting threefold to threefold (3-3), threefold to fourfold (3-4), and fourfold to fourfold (4-4) coordinated atoms. These bond lengths become larger going from 3-3 to 4-4 coordinated atoms, explaining the increase of the average nearest-neighbor distance with the percentage of fourfold coordination. Taking the average over the full set of models, we find 1.41, 1.50, and 1.57 Å for 3-3, 3-4, and 4-4 bond distances, respectively, in excellent agreement with the values derived for a fully *ab initio* model of *a*-C (1.41, 1.50, and 1.58 Å).[11] We determined the ring statistics for our model structures using the shortest path criterion introduced by Franzblau.[79] Both three- and four-membered rings occur in our models in agreement with experimental evidence,[3,4] and in concentrations similar to those found for models generated by first-principles methods.[11,14]

C. Calculated carbon 1*s* core-level shifts

We calculated C 1*s* core-level shifts including core-level relaxation effects for all the atoms in our model structures.

TABLE III. Structural properties of the model structures generated in this work: number of atoms in the supercell ($\mathcal{N}$), atomic density (ρ), average nearest-neighbor distance (d_{NN}), distribution of ring sizes (scaled to $\mathcal{N}=128$), and the percentage of threefold- (N_3), and fourfold- (N_4) coordinated atoms. The coordination is defined using a cut-off distance of 1.9 Å. The last column gives the calculated separation (Δ) between the average C 1*s* core-level shifts of three- and fourfold coordinated atoms.

			Number of rings							
$\mathcal{N}$	ρ (g/cm^3)	d_{NN} (Å)	3	4	5	6	7	N_3 (%)	N_4 (%)	Δ (eV)
128	1.77	1.46	2	5	35	17	6	75	21	0.96
64	2.01	1.48	0	2	36	20	6	78	22	1.15
64	2.15	1.45	6	4	26	18	12	81	19	1.26
128	2.21	1.49	3	8	39	24	13	55	43	0.94
64	2.40	1.53	8	10	56	20	20	34	66	0.66
64	2.59	1.54	4	20	44	24	16	31	67	0.93
128	2.63	1.53	4	17	53	23	32	25	72	1.00
64	3.03	1.57	0	14	68	44	38	6	94	1.12

Using the calculated values of the core-level shifts, we then simulated the XPS spectra adopting a Gaussian broadening of 1.0 eV, which corresponds to the experimental resolution in our experimental setup. Because our calculation only provides us with relative shifts, we took, for each model structure, the average shift of threefold-coordinated atoms as reference. Figure 3 displays the simulated C 1*s* core-level spectra for the three 128-atom model structures. The contributions from threefold- and fourfold-coordinated atoms are given separately. The small contributions from twofold-coordinated atoms are also indicated. As expected from the relative position of the C 1*s* line in diamond and graphite, the peaks associated with fourfold-coordinated atoms are located at higher binding energies. As can be seen in Fig. 3, the contributions from threefold- and fourfold-coordinated atoms result in well-separated, almost symmetric peaks. The different number of threefold- and fourfold-coordinated atoms is therefore responsible for the overall asymmetry of the simulated XPS line. Considering our complete set of models, we found that the dominant weight moves from the low- to the high-binding-energy side with increasing atomic density, in accord with experimental observations (Sec. II B).

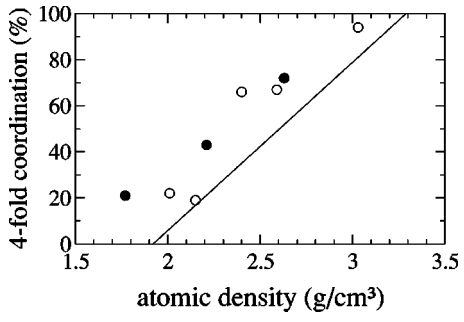

FIG. 4. Calculated percentage of fourfold-coordinated atoms as a function of atomic density. The model structures with 64 and 128 carbon atoms in the periodic supercell are indicated by empty and full circles, respectively. The line displays the empirical relationship from Ref. 6, given in Eq. (2).

The separation Δ between the average shift for threefold- and fourfold-coordinated atoms is given in Table III. For the three model structures with 128 atoms in the supercell, we found in all cases a separation of about 1.0 eV, which suggests that this value does not depend significantly on the atomic density. This result is in good agreement with our measured peak separation of 0.9 eV (see Table I). The model structures with 64 atoms show more scattered values of Δ, which, however, also average to 1.0 eV. We attribute this larger spread in Δ to strain effects associated with the smaller size of the models with only 64 atoms. Our results strongly support a decomposition of the C 1*s* core-level spectrum into two contributions,[33] and oppose the use of a third one as done in some analyses.[32,35] Note that, in Ref. 35, the use of a third contribution led to a sp^2-sp^3 peak separation of 0.55 eV, much lower than both our experimental data (0.9 eV) and theoretical estimates (1.0 eV).

The core-level shift can be decomposed into two different contributions. The initial-state shift, which is a strictly local property and is associated with the potential, and the contribution from core-hole relaxations. Shifts in the initial-state approximation can be obtained by the variation of the expectation value of the local potential on the atomic C 1*s* wave function.[61] We estimated the initial-state shifts by averaging the local potential on a sphere centered on the nuclei. We chose a sphere radius of 0.27 a.u. corresponding to the extent of the atomic C 1*s* wave function. In Fig. 5, we plot the core-level shifts for the model structure with $\rho=2.21$ g/cm^3 versus their respective initial-state values. We observe two important points. First, core-hole relaxation effects account for about 30% of the shift. Second, initial and final shifts scale linearly. The proportionality constant does not appear to depend on the coordination of the C atoms. A linear relationship is also found for the other model structures. Such a proportionality was also observed in other studies.[60–72]

The higher binding energy of fourfold-coordinated with respect to threefold-coordinated C atoms can be understood within an initial-state picture. The four electrons in the sp^3 orbitals of fourfold-coordinated atoms have an average dis-

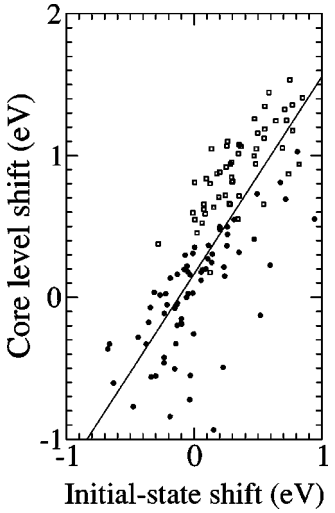

FIG. 5. Relation between C 1*s* core-level shifts calculated including core-hole relaxation, and those obtained using the initial-state approximation for the 128-atom model structure of *a*-C with an atomic density of 2.21 g/cm^3. Shifts associated with threefold- and fourfold-coordinated atoms are indicated by filled circles and open squares, respectively. The shifts on both axes are given with respect to the average value calculated for threefold-coordinated atoms. The solid line is a linear fit to all calculated points.

tance from the corresponding atomic core which is larger than that of the electrons of threefold-coordinated atoms (cf. Sec. III B). The higher potential at the core of threefold-coordinated atoms leads to a lower binding energy than for fourfold-coordinated atoms, as can be seen in our theoretical results. Core-hole relaxations also contribute to increasing the separation between C 1*s* core levels of threefold- and fourfold-coordinated atoms. In fact, screening is more effective at sp^2 sites, where the potential is higher (Fig. 5).

Considering the important overlap between calculated shifts resulting from threefold- and fourfold-coordinated atoms, it is of interest to analyze the corresponding bonding configurations. Focusing on threefold-coordinated C atoms with high C 1*s* binding energies, we often identified local structures in which the C atom has moved out of the plane of its nearest neighbors, towards an sp^3-like hybridization. At similar binding energies, we also found fourfold-coordinated C atoms with three nearest neighbors forming bond angles close to 120°, suggesting an sp^2-like hybridization. Therefore, although the core-level shifts of most C atoms is determined by the coordination number, these considerations indicate that in *a*-C samples there is a continuous distribution of hybridization states from pure sp^3 to pure sp^2, and that the relation between coordination and hybridization is sometimes subject to ambiguity.

IV. CONCLUSION

We have addressed C 1*s* core-level shifts in amorphous carbon, both experimentally and theoretically. In the experimental part of our investigation, we measured C 1*s* core-level spectra on samples of various atomic densities. We decomposed the spectra into two contributions, which we attributed to sp^2- and sp^3-hybridized C atoms. The separation between the sp^2 and sp^3 peaks was derived to be 0.9 eV, independent of atomic density. From the relative intensities of the two peaks, we estimated the percentage of sp^2- and sp^3-hybridized C atoms. We showed that these estimates are fully consistent with EELS measurements taken on the same samples. Because the penetration depth in EELS measurements is larger than in XPS, these results indicate that, for the density range we considered, surface effects do not significantly affect the sp^2/sp^3 hybridization ratio obtained from XPS data.

In the theoretical part of the work, we calculated C 1*s* core-level shifts within a first-principles framework, using a series of model structures generated by a molecular dynamics approach. This calculation showed that the C 1*s* shifts associated with threefold, and fourfold-coordinated atoms give rise to distinct contributions. The calculated separation between the average shifts of threefold- and fourfold coordinated atoms is 1.0 eV, in good agreement with our measured value of 0.9 eV. Furthermore, the calculated separation is independent of the atomic density of the model structures, as found experimentally. Therefore, this theoretical investigation provides a firm basis (i) for decomposing the C 1*s* photoelectron spectrum in terms of two components, and (ii) for their assignment to three- and fourfold coordinations, corresponding to sp^2- and sp^3-hybridized atoms. Hence, our results demonstrate that x-ray photoelectron spectroscopy reliably gives the sp^2/sp^3 hybridization ratio from the intensities of the two components in the C 1*s* spectrum.

ACKNOWLEDGMENTS

E.R. acknowledges useful interactions with Dr. F. Comin, Professor J. Chevrier, Professor M. Sancrotti, and all members of the Surface Science Laboratory at ESRF in Grenoble. This work was supported in part by the Swiss National Science Foundation under Grant Nos. 21-49697.96 (R.H. and A.B.) and 620-57850.99 (A.P.). The calculations were performed on an Origin 2000 of the Ecole Polytechnique Fédérale of Lausanne (EPFL) and on the NEC-SX4 of the Swiss Center for Scientific Computing (CSCS) in Manno.

*Electronic address: Rainer.Haerle@epfl.ch
†Electronic address: Elisa.Riedo@epfl.ch

[1] See J. Robertson, Prog. Solid State Chem. **21**, 199 (1991) for an overview.
[2] Fang Li and Jeffrey S. Lannin, Phys. Rev. Lett. **65**, 1905–1908 (1990).
[3] P. H. Gaskell, A. Saeed, P. Chieux, and D. R. McKenzie, Phys. Rev. Lett. **67**, 1286 (1991).
[4] K. W. R. Gilkes, P. H. Gaskell, and J. Robertson, Phys. Rev. B **51**, 12 303 (1995).
[5] Y. Lifshitz, Diamond Relat. Mater. **5**, 388 (1996); **8**, 1659 (1999).
[6] A. C. Ferrari *et al.*, Phys. Rev. B **62**, 11 089 (2000).

[7] G. Galli, R. Martin, R. Car, and M. Parrinello, Phys. Rev. Lett. **62**, 555 (1989); Phys. Rev. B **42**, 7470 (1990).
[8] C. Z. Wang, K. M. Ho, and C. T. Chan, Phys. Rev. Lett. **70**, 611 (1993).
[9] T. Frauenheim, P. Blaudeck, U. Stephan, and G. Jungnickel, Phys. Rev. B **48**, 4823 (1993).
[10] D. A. Drabold, P. A. Fedders, and P. Stumm, Phys. Rev. B **49**, 16 415 (1994).
[11] N. A. Marks, D. R. McKenzie, B. A. Pailthorpe, M. Bernasconi, and M. Parrinello, Phys. Rev. Lett. **76**, 768 (1996).
[12] C. Z. Wang and K. M. Ho, in *Covalently Bonded Disordered Thin-Film Materials*, edited by M. P. Siegal, J. E. Jaskie, W. Milne, and U. McKenzie, MRS Symposia Proceedings No. 498 (Materials Research Society, Pittsburgh, 1998), p. 498.
[13] R. Haerle, A. Baldereschi, and G. Galli, Appl. Phys. Lett. **75**, 1718 (1999); J. Non-Cryst. Solids **266–269**, 740 (2000).
[14] D. G. McCulloch, D. R. McKenzie, and C. M. Goringe, Phys. Rev. B **61**, 2349 (2000).
[15] C. Z. Wang, K. M. Ho, M. D. Shirk, and P. A. Molian, Phys. Rev. Lett. **85**, 4092 (2000).
[16] T. W. Scharf, R. D. Ott, D. Yang, and J. A. Barnard, J. Appl. Phys. **85**, 3142 (1999).
[17] H. Park, Y. K. Hong, J. S. Kim, C. Park, and J. K. Kim, Appl. Phys. Lett. **69**, 779 (1996).
[18] M. Chhowalla, J. Robertson, C. W. Chen, S. R. P. Silva, C. A. Davis, G. A. J. Amaratunga, and W. I. Milne, J. Appl. Phys. **81**, 139 (1997).
[19] Y. Lifshitz, in *The Physics of Diamond*, edited by A. Paoletti and A. Tucciarone, International School of Physics E. Fermi Vol. 135 (IOS, Amsterdam, 1997).
[20] A. Grill, Diamond Relat. Mater. **8**, 428 (1999).
[21] G. Comelli, J. Stör, J. Robinson, and W. Park, Phys. Rev. B **38**, 7511 (1988).
[22] P. J. Fallon, V. S. Veerasamy, C. A. Davis, J. Robertson, G. A. J. Amaratunga, W. I. Milne, and J. Koskinen, Phys. Rev. B **48**, 4777 (1993); **49**, 2287(E) (1994).
[23] E. Grossman, G. D. Lempert, J. Kulik, D. Marton, J. W. Rabalais, Y. Lifshitz, Appl. Phys. Lett. **68**, 1214 (1996).
[24] A. J. Papworth *et al.*, Phys. Rev. B **62**, 12 628 (2000).
[25] S. D. Berger, D. R. McKenzie, and P. J. Martin, Philos. Mag. Lett. **57**, 285 (1988).
[26] P. J. Fallon and L. M. Brown, Diamond Relat. Mater. **2**, 1004 (1993).
[27] D. Muller, D. R. McKenzie, and B. H. Pailthorpe, Phys. Rev. Lett. **67**, 773 (1991).
[28] M. A. Tamor and W. C. Vassell, J. Appl. Phys. **76**, 3823 (1994).
[29] P. J. Honeybone, R. J. Newport, J. K. Walters, W. S. Howells, and J. Tomkinson, Phys. Rev. B **50**, 839 (1994).
[30] K. C. Bastillo, M. A. Petrich, and J. A. Reimer, Chem. Mater. **2**, 202 (1990).
[31] H. Pan, M. Pruski, B. C. Gerstain, F. Li, and J. S. Lannin, Phys. Rev. B **44**, 6741 (1991).
[32] S. T. Jackson and R. G. Nuzzo, Appl. Surf. Sci. **90**, 195 (1995).
[33] J. Diaz, G. Paolicelli, S. Ferrer, and F. Comin, Phys. Rev. B **54**, 8064 (1996).
[34] P. Mérel, M. Tabbal, M. Chaker, S. Moisa, and J. Margot, Appl. Surf. Sci. **136**, 105 (1998).
[35] A. K. Sharma, R. J. Narayan, J. Narayan, and K. Jagannadham, Mater. Sci. Eng., B **77**, 139 (2000).
[36] E. Riedo, F. Comin, J. Chevrier, F. Schmithusen, S. Decossas, and M. Sancrotti, Surf. Coat. Technol. **125**, 124 (2000).
[37] P. Reinke and P. Oelhafen, Phys. Rev. B **56**, 2183 (1997); **60**, 15 772 (1999).
[38] A. A. Voevodin, M. S. Donley, and J. S. Zabinski, Surf. Coat. Technol. **92**, 1 (1997); **92**, 42 (1997).
[39] Y. Lifshitz, S. R. Kasi, J. W. Rabalais, and W. Eckstein, Phys. Rev. B **41**, 10 468 (1990).
[40] S. Uhlmann, T. Frauenheim, and Y. Lifshitz, Phys. Rev. Lett. **81**, 641 (1998).
[41] Pappas, K. Saenger, J. Bruley, W. Krakow, J. Cuomo, T. Gu, and R. Collins, J. Appl. Phys. **71**, 5675 (1992).
[42] C. D. Wagner, W. M. Riggs, L. E. Davis, J. F. Moudler, and G. E. Muilenberg, *Handbook of X-Ray Photoelectron Spectroscopy* (Perkin-Elmer).
[43] S. Doniach and M. Sunjic, J. Phys. C **3**, 285 (1970).
[44] We also fitted the measured C 1*s* core-level spectra using a combination of Gaussian and Lorentzian contributions for the sp^2 peak, instead of the Doniach-Sunjic function. For the samples with $I_L=1$ and 12 J/cm^2, this leads to a small change of the fourfold percentage from 34% to 37% and from 53% to 55%, respectively. We decided to use the Doniach-Sunjic function in our fits, because of the better agreement with EELS data.
[45] C. T. Chen and F. Sette, Phys. Scr. **31**, 119 (1990).
[46] C. Ronning, H. Feldermann, R. Herk, H. Hofsaess, P. Reinke, and J. U. Thiele, Phys. Rev. B **58**, 2207 (1998).
[47] D. A. Shirley, Phys. Rev. B **5**, 4709 (1972).
[48] In the case of the sample generated with a laser fluence of 1 J/cm^2, the fit with free parameters gave very different FWHM's for the two components (1.70 and 1.25 eV for the sp^3 and sp^2 components, respectively), and imposing equal FWHM's gave unsatisfactory fits. In this case, we therefore estimated the errors by fixing the FWHM of the sp^2 component at 1.25 eV.
[49] Y. Mizokawa, T. Miyasato, S. Nakamura, K. M. Geib, and C. W. Wilmsen, J. Vac. Sci. Technol. A **5**, 2809 (1987).
[50] J. F. Morar, F. J. Himpsel, G. Hollinger, J. L. Jordan, G. Hughes, and F. R. McFeely, Phys. Rev. B **33**, 1340 (1986).
[51] R. F. Egerton, *Electron Energy-Loss Spectroscopy in the Electron Microscope* (Plenum, New York, 1986).
[52] M. P. Seah and W. A. Dench, Surf. Interface Anal. I (1979).
[53] M. S. Tang, C. Z. Wang, C. T. Chan, and K. M. Ho, Phys. Rev. B **53**, 979 (1996).
[54] C. Xu, C. Z. Wang, C. T. Chan, and K. M. Ho, J. Phys.: Condens. Matter **4**, 6047 (1992).
[55] J. Tersoff, Phys. Rev. B **39**, 5566 (1989).
[56] R. Car and M. Parrinello, Phys. Rev. Lett. **55**, 2471 (1985).
[57] A. Pasquarello, K. Laasonen, R. Car, C. Lee, and D. Vanderbilt, Phys. Rev. Lett. **69**, 1982 (1992); K. Laasonen, A. Pasquarello, R. Car, C. Lee, and D. Vanderbilt, Phys. Rev. B **47**, 10 142 (1993).
[58] J. P. Perdew and Y. Wang, Phys. Rev. B **46**, 12 947 (1992).
[59] D. Vanderbilt, Phys. Rev. B **41**, 7892 (1990).
[60] E. Pehlke and M. Scheffler, Phys. Rev. Lett. **71**, 2338 (1993).
[61] A. Pasquarello, M. S. Hybertsen, and R. Car, Phys. Rev. B **53**, 10 942 (1996).
[62] A. Pasquarello, M. S. Hybertsen, and R. Car, Phys. Rev. Lett. **74**, 1024 (1995).
[63] A. Pasquarello, M. S. Hybertsen, and R. Car, Phys. Rev. B **53**, 10 942 (1996).

[64] A. Pasquarello, M. S. Hybertsen, and R. Car, Phys. Scr. **T66**, 118 (1996).
[65] A. Pasquarello, M. S. Hybertsen, and R. Car, J. Vac. Sci. Technol. **14**, 2809 (1996).
[66] A. Pasquarello, M. S. Hybertsen, and R. Car, Phys. Rev. B **54**, R2339 (1996).
[67] A. Pasquarello, M. S. Hybertsen, G.-M. Rignanese, and R. Car, in *Fundamental Aspects of Ultrathin Dielectric on Si-Based Devices*, edited by E. Garfunkel, E. Gusev, and A. Vul (Kluwer, Dordrecht, 1998), p. 89.
[68] K. Raghavachari, A. Pasquarello, J. Eng, Jr., and M. S. Hybertsen, Appl. Phys. Lett. **76**, 3873 (2000).
[69] G.-M. Rignanese, A. Pasquarello, J.-C. Charlier, X. Gonze, and R. Car, Phys. Rev. Lett. **79**, 5174 (1997).
[70] G.-M. Rignanese and A. Pasquarello, Appl. Phys. Lett. **76**, 553 (2000).
[71] G.-M. Rignanese and A. Pasquarello, Phys. Rev. B **63**, 075307 (2001).
[72] A. Palma, A. Pasquarello, and R. Car, Phys. Rev. B (to be published).
[73] A. Catellani, G. Galli, and F. Gygi, Appl. Phys. Lett. **72**, 1902 (1998).
[74] Y. Travaly, D. Vanderbilt, and X. Gonze, Phys. Rev. B **61**, 7716 (2000).
[75] A. A. Bakke, H. W. Chen, and W. L. Jolly, J. Electron Spectrosc. Relat. Phenom. **20**, 333 (1980).
[76] L. Pedocchi, N. Russo, and D. R. Salahub, Phys. Rev. B **47**, 12 992 (1993).
[77] N. A. Marks, Phys. Rev. B **56**, 2441 (1997).
[78] R. Haerle, Ph.D. thesis, Ecole Polytechnique Fédérale de Lausanne (EPFL), 2002.
[79] D. S. Franzblau, Phys. Rev. B **44**, 4925 (1991).
[80] F. J. Himpsel, F. R. McFeely, A. Taleb-Ibrahimi, J. A. Yarmoff, and G. Hollinger, Phys. Rev. B **38**, 6084 (1988).